The International Journal of Advanced Manufacturing Technology (2022) 122:499–512
https://doi.org/10.1007/s00170-022-09361-3

APPLICATION

# A comparative study on surface topography and microhardness of laser polished-hardened AISI D2 tool steel

Zuofa Liu[1] · Jie Zhou[1] · Hang Wang[1] · Qiuyun Wang[1] · Qiang Liang[2] · Yongliang Li[2]

Received: 21 September 2021 / Accepted: 10 May 2022 / Published online: 18 June 2022


## Abstract

Although a laser beam with a small diameter (< 1 mm) can significantly improve surface morphology, the polishing efficiency is very low, and the improvement of surface hardness is negligible. In this work, a novel laser polishing-hardening (LPH) method with integration and high efficiency for the treatment of AISI D2 tool steel using a large-size laser beam ($\Phi$2.8 mm) was proposed, and the effects of laser hardening (LH), laser polishing (LP), and LPH treatments on the surface topography and microhardness were examined. The results show that the LH method had a negligible effect on the surface roughness of the treated sample, while the surface roughness *Ra* of LP and LPH specimens was reduced by 74.6% and 80.9%, respectively, indicating that the milled surface topography had been significantly improved, especially LPH was more effective in reducing the roughness. Besides, the polishing efficiency of LPH was 10 times that of the LP approach. In terms of hardness improvement, the near-surface microhardness of LH and LPH samples increased by 1.5 times and 1.3 times, respectively, and the effective hardened zone (EHZ) depth was 0.42 mm and 0.24 mm, respectively, demonstrating that these two laser processing methods had a beneficial effect on the cross-section microhardness of D2 tool steel, while the increase of LP on the microhardness was insignificant. The comprehensive analysis of the surface morphology and microhardness of the LPH specimen indicates that LPH was a feasible laser surface treatment method for D2 tool steel. On the premise of ensuring a high surface finish, the polishing efficiency can be remarkably improved, and the subsurface microhardness and EHZ depth of processed specimen can be also significantly increased, which provided a feasible idea for the application of laser surface treatment technology in industrial mold production.

**Keywords** AISI D2 tool steel · Surface topography · Microhardness · Laser polishing · Laser hardening · Strengthening mechanism

## 1 Introduction

As monochromatic radiation and directional non-contact heating source, the laser is extensively used in the surface engineering of metallic materials. Laser surface engineering methods of tool steel can be mainly divided into direct processes, which only need the generated heat, such as laser polishing (LP) and laser hardening (LH), and processes that need filler material, such as laser cladding (LC). Laser polishing is a method of melting a small amount of material in the near-surface zone of tool steel by laser irradiation to refine and homogenize the material structure and then improve the comprehensive performance such as surface roughness and wear resistance [1]. Similarly, laser hardening is also a common surface treatment technology using laser as a heating source. The material of the metal surface is heated to the austenitizing temperature by laser energy and then self-quenched to induce martensitic transformation on the surface, resulting in significant improvement of the surface hardness [2].

Laser cladding is a technology of using a high-energy–density laser beam to melt and rapidly solidify

This article is part of the Topical Collection: *New Intelligent Manufacturing Technologies through the Integration of Industry 4.0 and Advanced Manufacturing*

✉ Jie Zhou
zhoujie@cqu.edu.cn

[1] Chongqing Key Laboratory of Advanced Mold Intelligent Manufacturing, College of Materials Science and Engineering, Chongqing University, Chongqing 400044, China

[2] College of Mechanical Engineering, Chongqing Technology and Business University, Chongqing 400060, China

the cladding material and the substrate surface, leading to achieving the metallurgical bonding between the cladding layer and the substrate surface. Thus, the properties of the substrate surface can be remarkably improved, such as wear resistance, corrosion resistance, heat resistance, and oxidation resistance [3].

In recent years, considerable progress has been made in laser polishing metal surfaces. Krishnan and Fang [4] reported that under the optimal parameters, the average surface roughness of several metal materials could be decreased by 80%, and the processing efficiency could be also increased by an order of magnitude compared with manual polishing. Dai et al. [5] adopted the top-hat distribution laser beam with a diameter of 0.2 mm to reduce the initial surface roughness *Ra* of SKD 11 tool steel from 3.571 to 0.332 μm. Ukar et al. [6] developed a prediction method for the surface morphology of laser polishing and then conducted an experiment to verify its effectiveness on DIN 1.2379 tool steel. Ukar et al. [7] examined the influence of $CO_2$ laser and diode laser on the surface roughness and microstructure of DIN 1.2379 tool steel. Chang et al. [8] investigated the effect of laser energy on surface topography and the long-term performance of polished SKD 61 tool steel by applying a fiber laser. Guo et al. [9] optimized the LP process parameters of DF-2 tool steel by using the orthogonal design test method. Ma et al. [10] studied the polishing performance of fiber laser on the surface of as-received Ti-6Al-4 V. They found that the surface roughness of Ti-based alloys could be diminished to 1 μm. Pong-Ryol et al. [11] conducted laser micro-polishing experiments on two different surface forms of 316L stainless steel with a continuous wave laser beam. It was found that the surface roughness of the inclined plane and curved surface decreased by 56.4% and 57.3%, respectively. Kang et al. [12] developed a laser polishing technology with ultrasonic vibration, which realized the uniform heating of micro peaks and valleys on the 304 steel surface, and the surface morphology was remarkably improved. Zhou et al. [13] investigated the influence of laser polishing on the surface morphology of S316D tool steel by numerical simulation and experimental methods. The experimental results indicate that the initial surface roughness could be reduced to 0.764 μm, and the error between the actual molten and simulated pool depth was 5.3%. Lee et al. [14] polished the surface of the as-received Ti-6Al-4 V sample. The fatigue life of laser polished specimens was slightly longer than that of solid specimens due to the reduction of surface roughness.

In the above laser experiments, the metal surfaces were both polished using laser energy with a small spot diameter (< 1 mm). Although it can significantly reduce the metal surface roughness and improve the surface morphology, the polishing efficiency is very low. For example, it takes about 150 min to polish a plane with a size of 100 mm × 100 mm. In comparison with conventional manual polishing, it has insignificant advantages except for automation. Moreover, the degree of hardness improvement is negligible due to the small laser energy, and the effective hardening zone (EHZ) depth is only 20 ~ 40 μm, which cannot satisfy the functional requirements of industrial dies and molds.

At present, it has been well verified that high-power laser beams can be desirably adopted to remarkably increase the surface hardness of metallic materials. Muthukumaran and Babu [15] applied a 4-KW high-power diode laser to strengthen the surface of 2.5Ni-Cr–Mo steel. They found that there was strip martensite in the hardened zone, and the hardness increased to 700 HV, which was 3.5 times that of the base metal. Bande et al. [16] studied the effects of laser transformation hardening on the microhardness and structure of AISI 01 die steel. Akao et al. [17] found that the hardness of SKD 11 die steel treated by laser beam increased from 200 to 430 HV due to grain refinement and austenite dissolution. Amine et al. [18] employed a 9-kW CW $CO_2$ laser to study the effect on the microstructure and hardness of AISI D2 cold working tool steel. The investigation on the microhardness and gradient of laser hardened AISI 1045 carbon steel using response surface methodology was carried out by Chen et al. [19]. Lesyk et al. [20] developed a compound surface treatment approach of laser surface hardening and ultrasonic impact treatment and examined the influences of D2 die steel on surface morphology, hardness, and microstructure. Li et al. [21] compared the effects of laser hardening of AISI 1045 steel applying $CO_2$ laser and high-power diode laser. Dinesh Babu et al. [22] conducted laser transformation hardening on EN 25 carbon steel using a 2-KW CW laser system and investigated the effect of process parameters on hardening degree. Lee et al. [23] used a fiber laser as a heating source to enlarge the surface microhardness and wear resistance of H13 tool steel. Tobar et al. [24] established a three-dimensional numerical model of laser hardening of H13 die steel, which was confirmed by experiments. The results of experiment show that the measured hardness and depth distribution were well consistent with the numerical prediction.

To achieve the purpose of small surface roughness, high polishing efficiency, significant increases of subsurface microhardness, and EHZ depth, the surface of AISI D2 tool steel was treated using the laser energy with a large spot ($\Phi$2.8 mm). Besides, the comparison and analysis of LH, LP, and LPH on surface topography and microhardness were carried out to verify the feasibility of the proposed LPH method.

## 2 Materials and methods

### 2.1 Experimental materials

AISI D2 is a cold working tool steel with high wear resistance, hardenability, and thermal stability formed by

**Table 1** Chemical composition of AISI D2 (wt%)

| Elements | Cr | Mo | Mn | V | Si | C | Fe |
|---|---|---|---|---|---|---|---|
| AISI D2 (%) | 11.8 | 0.8 | 0.35 | 0.95 | 0.25 | 1.55 | Bal |

adding Cr, Mo, V, and other elements into carbon steel. It is extensively used in the manufacture of various automobile stamping dies with large sections, complex structures, and heavy working conditions, such as punching die, trimming die, edging die, and stretching die. In this work, D2 tool steel was supplied under annealed conditions and heated to 850 °C, then slowly cooled to 650 °C in the furnace at a rate of 10 °C/h, and then taken out and cooled in air. The surface microhardness of tool steel is 250 $HV_{500}$, and the main chemical composition is given in Table 1.

The dimension of the experimental sample was 200 mm × 50 mm × 20 mm. The initial surface of the specimen was prepared by the milling approach, and the detailed processing conditions are presented in Table 2. The same prepared surface was applied in all experiments of laser processing. Figure 1 shows the prepared surface topography. The roughness parameters were 2.617 μm *Ra*, 8.155 μm *Rz*, and 20.065 μm *Rt*, which can be regarded as a common semi-finished surface in the mold production industry.

## 2.2 Experimental procedures

Figure 2a illustrates the laser processing equipment, which is composed of a fiber-coupled diode laser, an optical transmission system, an integrated controller, a six-axis robot, and a shielding gas system. The fiber-coupled diode laser (Model LDM 3000–100) was developed by Laserline company with a wavelength of 900 ~ 1070 nm and an output peak power of 3000 W. The laser head was connected with an industrial robot (Model IRB 4600–40) developed by ABB

**Table 2** Processing parameters of initial specimen surface

| Items | Values |
|---|---|
| Processing tool | Ball-end mill |
| Processing trajectory | Zigzag |
| Tool diameter (mm) | 16 |
| Feed speed (mm/min) | 400 |
| Rotation speed (r/min) | 3000 |
| Radial depth (mm) | 0.2 |
| Axial depth (mm) | 0.2 |
| Stepover (mm) | 0.4 |

corporation to move, which can realize a six-axis linkage. The laser processing experiments were conducted at a 45° angle concerning the milling direction and adopted the zigzag scanning trajectory to process the entire surface, as presented in Fig. 2b.

To study the influences of laser surface treatment technologies like LH, LP, and LPH on the surface morphology and hardness of D2 tool steel, a series of laser processing experiments were carried out on the milled surface with three different types of industrial laser heads. In the LH test, the laser head with a spot size of 13 mm × 6 mm was adopted, which was especially used for laser hardening of the tool steel surface. Besides, the laser energy distribution was flat-top, and there was no shielding gas during the experiment. A laser head with a spot diameter of 0.1 mm was applied in the LP experiment, which was widely used for laser polishing metal material, and the laser energy was defined as Gaussian distribution. In the compound experiment of laser polishing and hardening, a laser head with a spot diameter of 2.8 mm was used, and the laser energy presented a Gaussian distribution. In LP and LPH experiments, Ar and $N_2$ (99.999% purity) was directly sprayed on the sample surface at the rate of 0.5 L/s to prevent the processed surface from oxidation, respectively. Table 3 lists the processing parameters of LH, LP, and LPH experiments.

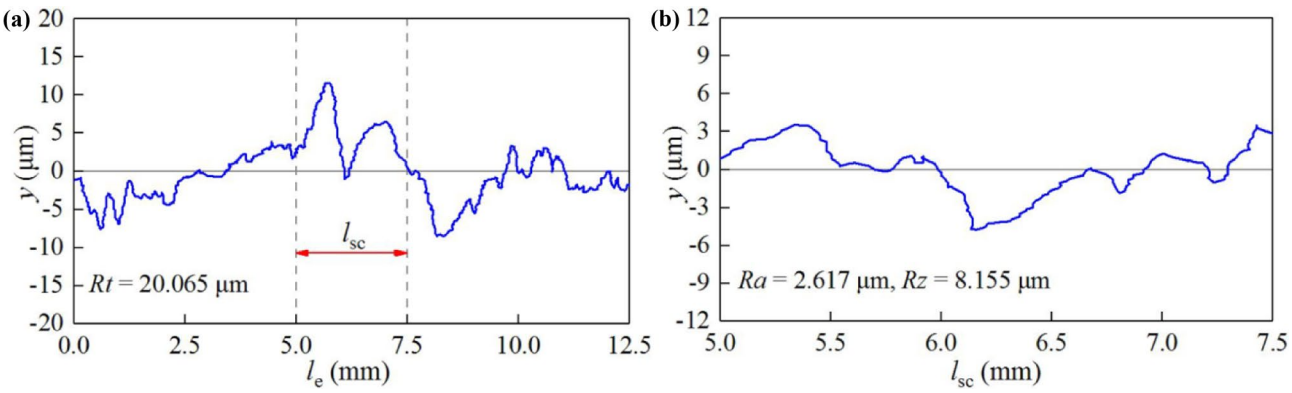


**Fig. 1** Prepared surface topography: (**a**) primary profile curve; (**b**) roughness profile curve

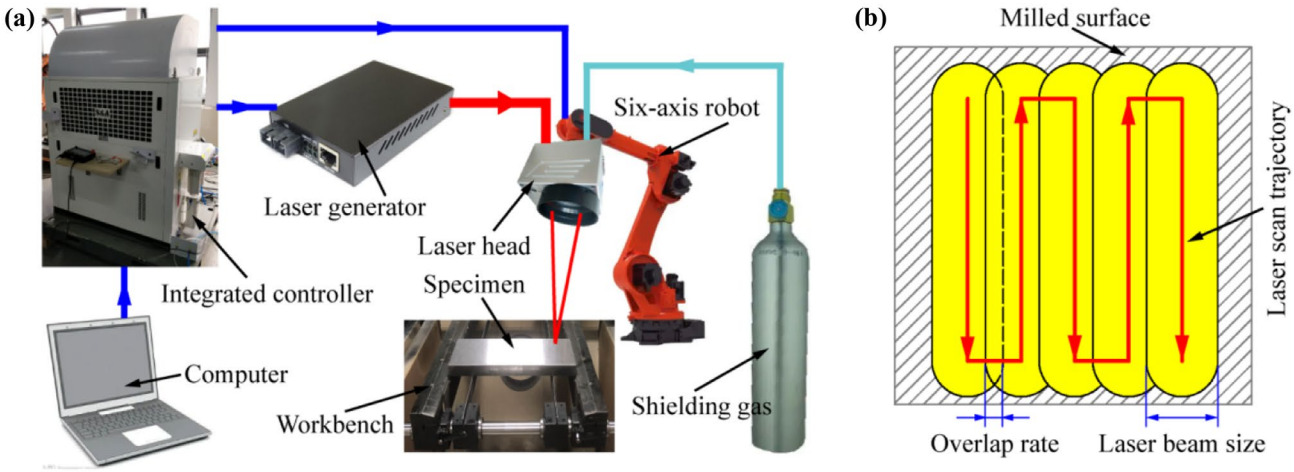


**Fig. 2** Schematic diagram of laser processing equipment: (**a**) laser system; (**b**) laser scanning trajectory

## 2.3 Surface topography

The surface morphology illustrates the shape of hills and dales, and its amplitude and frequency determine the surface quality, which is widely presented as roughness. According to the physical characteristic of measurement, different parameters can be adapted to measure surface roughness. For example, surface roughness is usually evaluated by applying the following three parameters in the mold and die industry, as shown in Fig. 3;

1. The arithmetical mean deviation of profile *Ra*: the arithmetical mean of the absolute value of the profile departure within a section length, which can be calculated as

$$Ra = \frac{1}{l_{sc}} \int_0^{l_{sc}} |y(x)| \mathrm{d}x \tag{1}$$

   where $l_{sc}$ is a section length and $y$ is profile departure.
2. The maximum height of profile *Rz*: the sum of height of the largest profile hill height and the largest profile dale depth within a section length, which can be described as

$$Rz = \max\left\{y_{pi}(x)\right\} + \max\left\{\left|y_{vj}(x)\right|\right\} \quad i = 1, 2, ....; j = 1, 2, ...; 0 \le x \le l_{sc} \tag{2}$$

   where $y_{pi}$ is the profile hill height and $y_{vj}$ is the profile dale depth.
3. The total height of profile *Rt*: the sum of height of the largest profile hill height and the largest profile dale depth within the evaluation length, which can be expressed as

$$Rt = \max\left\{y_{pi}(x)\right\} + \max\left\{\left|y_{vj}(x)\right|\right\} \quad i = 1, 2, ....; j = 1, 2, ...; 0 \le x \le l_e \tag{3}$$

   where $l_e$ is the evaluation length, which can be defined as

$$l_e = n \times l_{sc} \quad n = 1, 2, .... \tag{4}$$

The surface topography of the processed samples was analyzed by a Leica DVM6S hyperfocal optical microscope (HOM), the surface roughness was measured with a TIME-3221 profilometer, and the primary profile curve and roughness profile curve were extracted using the TIME-3R-2.0 software. The primary profile is the profile after low-pass filtering of the measured profile where the wavelength components below a cut-off wavelength are removed. The roughness profile is the profile after high-pass filtering of

**Table 3** Laser surface processing parameters

| Approaches | Parameters |
|---|---|
| LH | Spot shape: rectangle, spot size: 13 mm × 6 mm, laser energy density: 282 J/cm.$^2$, defocus: 0, scanning trajectory: single pass, no shielding gas |
| LP | Spot shape: circular, spot size: $\Phi$0.1 mm, laser energy density: 3333 J/cm.$^2$, defocus: 3 mm, scanning overlap rate: 50%, scanning trajectory: multi-pass and zigzag, shielding gas: Ar (99.999% purity), shielding gas flow rate: 0.5 L/s |
| LPH | Spot shape: circular, spot size: $\Phi$2.8 mm, laser energy density: 1786 J/cm.$^2$, defocus: 0, scanning overlap rate: 60%, scanning trajectory: multi-pass and zigzag, shielding gas: $N_2$ (99.999% purity), shielding gas flow rate: 0.5 L/s |

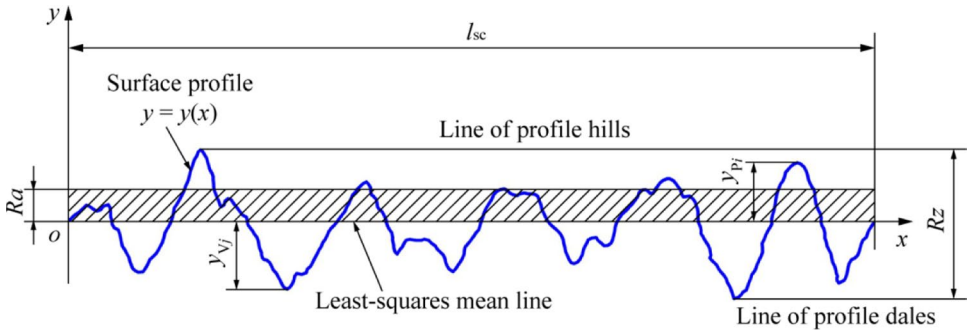


**Fig. 3** Parameters for evaluating surface roughness

the primary profile where the longer wavelength components (which are more relevant to the waviness profile) are removed. The roughness section length ($l_{sc}$) corresponds to the cut-off wavelength of this high-pass filter, and the roughness evaluation length ($l_e$) is usually 5 times the roughness section length. Based on the international standard of rules and procedures for the assessment of surface texture (ISO 21920–3: 2021), when the section length is defined as 0.8 mm, the evaluation length is 4.0 mm. And, when the section length is defined as 2.5 mm, the evaluation length is 12.5 mm. Besides, five different surface roughness measurements were made for each experiment to obtain an accurate value.

## 2.4 Cross-section microhardness

The metallographic specimens with the dimensions of 10 mm × 10 mm × 5 mm were cut by the wire electrical discharge machine (WEDM) in the direction perpendicular to the laser scanning on the treated D2 tool steel. And, the cross-sections of the processed specimens were mechanically polished and etched with a 4% nitric acid + 96% alcohol solution. The analysis and observation of the microstructure in the cross-section were conducted by using a Leica DMILM optical microscope.

Microhardness measurements of the cross-section were carried out using an HV-1000 Vickers microhardness tester with a 500 g applied load for 15 s and were taken at an increment of 0.1 mm in the vertical direction. The hardness values were the average of three readings taken along a centerline from the surface of the sample towards the center at the same depth from the surface.

D2 tool steel was analyzed by the XRD method to study whether new phases precipitated after laser treatments. The equipment used in this study was an X-ray diffractometer (Model DX-2700B). The scanning angle range was 20 ~ 90°, the step angle was 0.02°, and the sampling time was 0.5 s. The XRD pattern of the sample was compared with the standard database (PDF card) from the aspects of diffraction fringes, matching degree, and cell parameters to determine the phase composition of the experimental sample.

Figure 4 shows three different regions in the cross-sectional microstructure of each laser-treated specimen, namely remolten zone (RZ), transformation hardened zone (THZ), and substrate zone (SZ). RZ was represented as the zone had undergone melting and re-solidification. THZ represented the region where the phase transformation occurred under the influence of laser energy, resulting in a significant increase in hardness. SZ indicated the original material, which was not affected by the laser application. The hardened zone (HZ) depth of the cross-section was defined as the vertical distance from the sample surface to the bottom of the semi-circular THZ, which was composed of the EHZ depth and the heat-affected zone (HAZ) depth. According to the international standard on the determination of the effective depth of hardening (ISO 18203), the EHZ depth is the vertical distance from the test surface to the limiting hardness, and the limiting hardness of D2 tool steel is 458 HV. The width of the hardened region was the width of the hardness increase of the material on the treated specimen surface. As the multi-pass strategy is extensively used for laser processing of parts and tools in actual industrial production, the transversal hardening zone width is not considered in this work. For the depth measurement of each zone, the average value of three measurements was adopted.

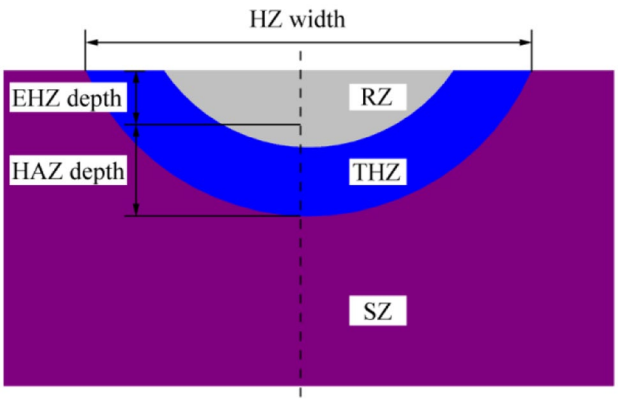


**Fig. 4** Schematic diagram of processed cross-section structure

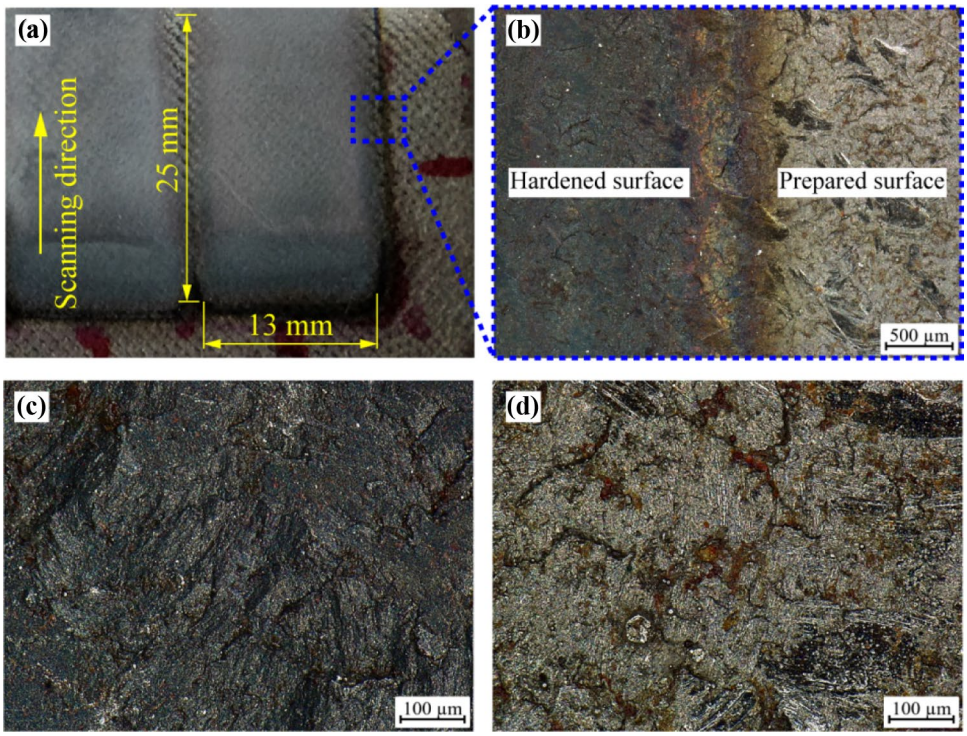


**Fig. 5** 3D surface morphologies of LH specimen: (**a**) macroscopic image; (**b**) HOM image; (**c**), (**d**) higher-magnification HOM images of hardened and initial surface

## 3 Experimental results

### 3.1 Effects of LH on specimen characteristics

Figure 5 displays the three-dimensional surface morphology of the laser hardened sample. The macroscopic image is illustrated in Fig. 5a, where the black rectangular area has been subjected to LH. The treated surface is free of cracks, scars, and other obvious defects and remains flat. Figure 5b shows the HOM view of the division of the hardened and pre-prepared surfaces. It can be clearly observed that the processing tracks of the ball-end mill and the milling surface topography were mainly composed of semi-elliptical or hemispherical peaks with a regular distribution. Compared to the milled surface, the specimen surface after LH was light black. This is due to the experiment of LH performed in the atmosphere without shielding gas, which leads to oxidation. Figure 5c, d present higher-magnification HOM images of the hardened and initial zones, respectively. Melting metal did not appear on the sample surface due to the uniform distribution of the flat-top beam energy.

To further investigate the influence of laser beams on the surface topography of hardened specimens, the surface topography was characterized by a roughness profiler. The 2D surface topographies of the LH specimen are shown in Fig. 6. The arithmetical mean deviation *Ra* of the hardened profile was 2.468 μm, the maximum height *Rz* was 7.273 μm, and the total height *Rt* was 17.640 μm. In comparison with the initial surface roughness, the reduction rate of *Rt* was the largest (12.1%), indicating that the initial surface profile was hardly affected by laser hardening treatment.

The overall microstructure of the cross-section using LH is illustrated in Fig. 7a. The cross-section of the hardened specimen can be divided into two areas. The first one was a dark structure with a height of 700 μm on the subsurface, which was called the transformation hardening zone. This area was a regular rectangle. This can be explained that the distribution of flat-top laser beam was uniform, leading to the same energy

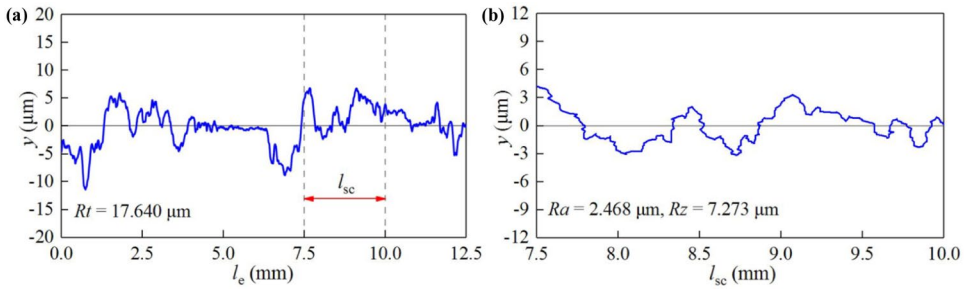


**Fig. 6** 2D surface morphologies of LH specimen: (**a**) primary profile curve; (**b**) roughness profile curve

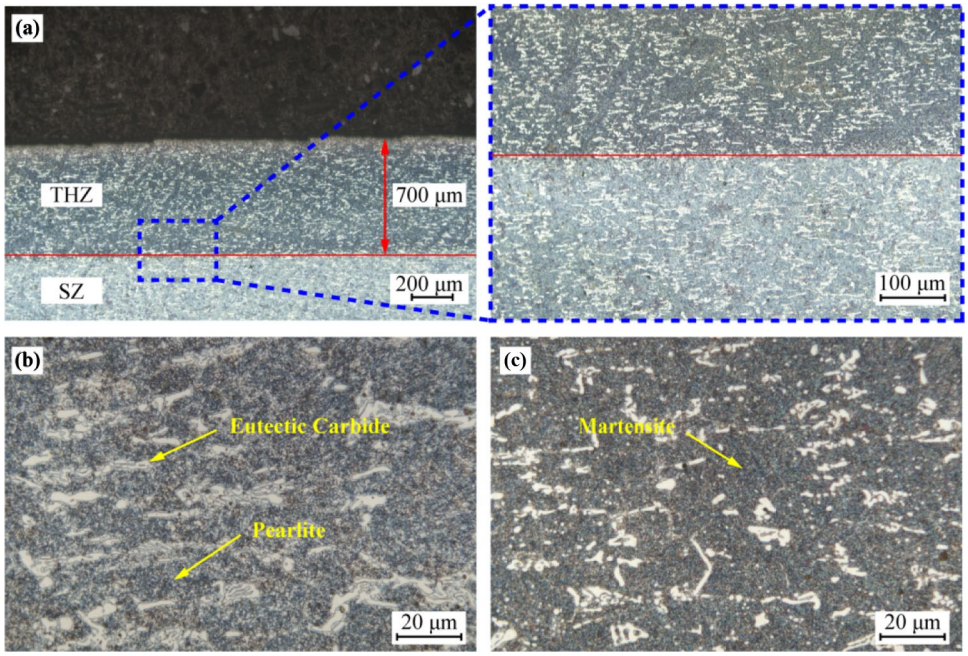


**Fig. 7** Cross-sectional microstructure using LH: (**a**) overall; (**b**) SZ; (**c**) THZ

absorbed by the sample surface in the horizontal direction. The other one was the brightly etched original substrate area, which was not affected by laser processing. Figure 7b presents the microstructure before laser hardening. A large number of aggregated and segregated eutectic carbides were distributed on the spheroidal pearlite matrix formed by spheroidizing annealing. The microstructure after LH is shown in Fig. 7c. It can be observed that the microstructure of D2 tool steel has changed significantly. The matrix structure converted from pearlite to martensite, and the size of eutectic carbide diminished remarkably. This is due to the laser energy irradiates on the metal surface, and the metal absorbs the laser radiation and converts it into heat. When the sample surface in the laser scanning area reaches the austenitizing temperature, considerable austenites have no time to grow up and directly transform into martensite during the rapid cooling process. In addition, with the rapid heating of the laser application, the eutectic carbide gradually dissolves, thereby its size reduces significantly.

Figure 8 shows the microhardness distribution of the hardened specimen. The material near the surface absorbed a large amount of laser energy in the LH processing. Due to its rapid cooling, the structure changed into martensite with fine grains, resulting in the hardness increasing to 634 $HV_{500}$. Compared to the initial hardness of 250 $HV_{500}$, the hardness of the hardened sample was increased by 153.6%. Moreover, the farther the material was from the surface, the less affected the laser energy, and the hardness decreased gradually. Under the action of the laser, the thickness of the material with remarkably improved hardness was 0.7 mm, which was consistent with the distribution of microstructure (see Fig. 7a). The thickness of the material whose microhardness reached the limiting hardness (458 $HV_{500}$) of D2 tool steel was 0.42 mm, indicating that the EHZ depth was 0.42 mm and HAZ depth was 0.28 mm.

The XRD patterns of the D2 tool steel surface before and after LH are displayed in Fig. 9. XRD results show that the original D2 steel consists of matrix phase $\alpha$-Fe and eutectic carbide $(Cr, Fe)_7C_3$. In addition to these two phases, new phases $(Cr_{2.5}Fe_{4.3}Mo_{0.1})C_3$ and $Fe_2O_3$ were produced on the sample surface after LH, where $(Cr_{2.5}Fe_{4.3}Mo_{0.1})C_3$ was a fine secondary carbide precipitated by laser and $Fe_2O_3$ was an oxide produced by oxidation reaction on the surface of D2 tool steel due to the absence of shielding gas.

## 3.2 Effect of LP on specimen characteristics

Figure 10 presents the 3D surface topography of the laser polished sample. The macro image is shown in Fig. 10a,

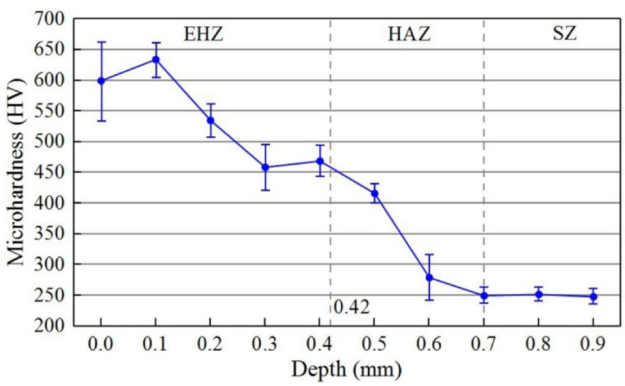


**Fig. 8** Microhardness distribution of LH subsurface

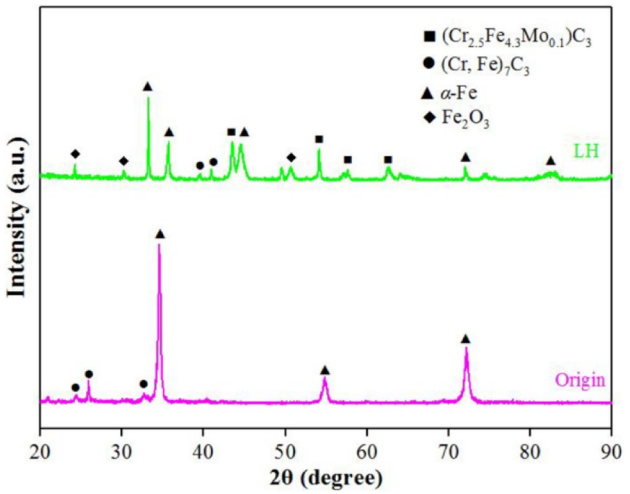


**Fig. 9** XRD patterns of D2 steel before and after LH

where the white bright rectangular area is treated by the LP approach. The laser beam and shielding gas (Ar) acted on the specimen surface at the same time during the experiment; thus, oxidation was hardly observed on the polished surface. The HOM view of the division of the polished and initial surfaces is displayed in Fig. 10b. The polished surface presented regular overlap characteristics due to the laser beam scanned the sample surface at a fixed overlap rate. Besides, the milling path of the sample surface had been replaced by the zigzag laser scanning path. Figure 10c, d illustrate higher-magnification HOM images of the polished and milled zones, respectively. When the laser acted on the sample, the material on the surface would absorb energy and convert it into heat, and thereby the surface would melt. Due to the effect of surface tension, the convex part on the surface would flatten. As the removal of the laser beam, the molten material would solidify again, leading to the roughness of the processed surface being reduced remarkably.

The 2D surface morphology of the polished specimen is presented in Fig. 11. Due to the laser beam scanned the sample surface at a fixed overlap rate of 50%, the polished surface profile showed a regular distribution law of hill and dale. The arithmetical mean deviation *Ra* of the polished profile was 0.666 μm, the maximum height *Rz* was 3.130 μm, and the total height *Rt* was 8.026 μm. In comparison with the initial milled surface, the reduction rate of *Ra* was the largest (74.6%), indicating that the surface roughness after laser polishing had been significantly improved and satisfied the requirements of industrial mold.

The cross-sectional microstructure using LP is shown in Fig. 12a. Unlike the laser-hardened specimen, the subsurface of the polished sample was a half-moon-shaped and white-bright remelting zone with a depth of 30 μm. It can be explained that the Gaussian distributed laser beam irradiated

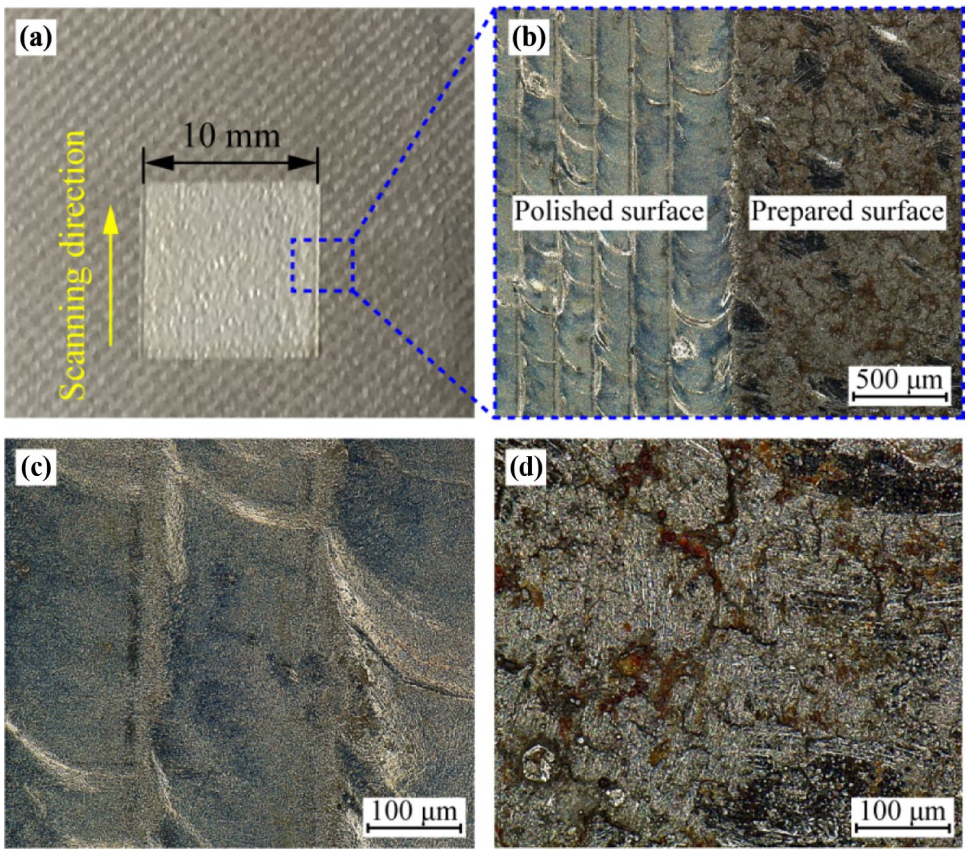


**Fig. 10** 3D surface morphologies of LP specimen: (**a**) macroscopic image; (**b**) HOM image; (**c**), (**d**) higher-magnification HOM images of polished and prepared surface

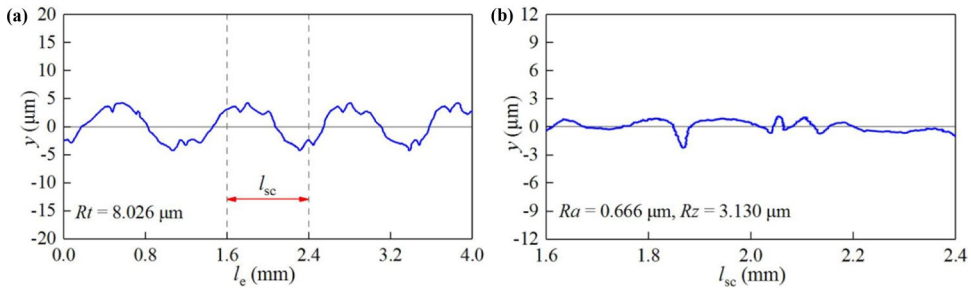


**Fig. 11** 2D surface morphologies of LP specimen: (**a**) primary profile curve; (**b**) roughness profile curve

on the specimen surface, which made the temperature of the sample surface raised to the melting temperature, then the thin layer of molten material in contact with the colder substrate will produce strong cooling, resulting in the achievement of re-solidification. It was in good agreement with the surface shallow melting (SSM) mechanism proposed by Ramos-Grez and Bourell [25].

Figure 12b illustrates the microhardness distribution of the polished specimen. The hardness of RZ was increased to 277 $HV_{500}$ by the martensitic transformation, which was only 10.8% higher than the initial hardness. It was far from the limiting hardness of D2 tool steel, indicating that laser polishing can only reduce the surface roughness and hardly achieve the purpose of hardening. With the increase of the distance from the surface, the microhardness decreased gradually. When the distance was larger than 0.3 mm, the microhardness was stable at 250 $HV_{500}$, demonstrating that the depth of the hardened layer after laser polishing was 0.3 mm.

XRD analysis was carried out on the polished sample to study the effect of laser polishing on the phase composition of the D2 tool steel surface. Figure 13 shows the XRD pattern. After laser polishing of D2 tool steel, in addition to the matrix phase $\alpha$-Fe corresponding to the three main diffraction peaks (110), (200), and (211) and the eutectic carbide $(Cr, Fe)_7C_3$ corresponding to the diffraction peaks (420) and (440), a new phase $(Cr_{2.5}Fe_{4.3}Mo_{0.1})C_3$ corresponding to the diffraction peak (412) was produced. Moreover, no oxide $Fe_2O_3$ was observed, indicating that the oxidation reaction was effectively prevented by the shielding gas.

## 3.3 Effect of LPH on specimen characteristics

Figure 14 shows the 3D surface morphologies of the processed specimen using LPH. The macroscopic image is given in Fig. 14a, where the yellow-bright rectangular area has been treated. It can be observed that the processed surface presented the regular micro-characteristics of peaks and valleys. This can be explained as the scanning strategy with a fixed overlap rate of 60% was adopted in the LPH experiment. Figure 14b displays the HOM view of the division of the processed and pre-prepared surfaces. Compared with the initial milling surface, the sample surface after laser scanning changed remarkably and became smoother. Figure 14c, d show higher-magnification HOM images of the processed and initial zones, respectively. Compared with the LP test, a laser spot with a diameter of 2.8 mm was adopted in the LPH experiment. It was obvious that the more laser energy gathered on the sample surface, the more molten material increased significantly.

The 2D surface morphology of LPH sample is shown in Fig. 15. The arithmetical mean deviation *Ra* of the processed profile was 0.499 μm, the maximum height *Rz* was 2.065 μm, and the total height *Rt* was 7.341 μm. Compared with the initial surface, *Ra* decreased the most (80.9%), demonstrating that LPH method can significantly reduce the milling surface roughness.

Figure 16a illustrates the overall microstructure using LPH. The cross-section can be divided into three areas. This first one was a half-moon-shaped and white-bright remelting zone with a depth of 300 μm, which was 10 times that of the polished specimen, as presented in Fig. 16b. This is because

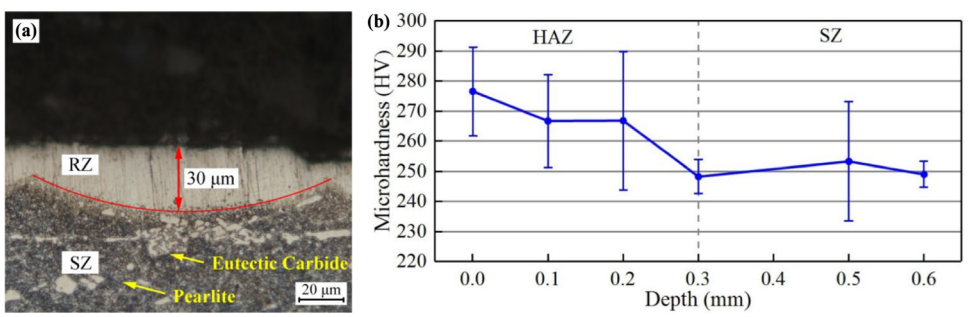


**Fig. 12** Cross-sectional characteristics using LP: (**a**) microstructure; (**b**) microhardness

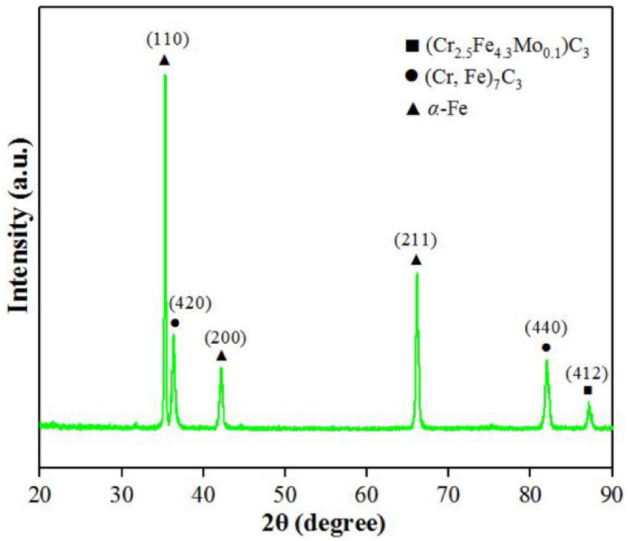


**Fig. 13** XRD pattern of D2 steel after LP

the laser beam in the LPH experiment did not defocus on the sample surface. The greater the energy absorbed by the sample, the deeper the remelting zone. This is consistent with the surface over melting (SOM) mechanism developed by Ramos-Grez and Bourell [25]. The second region was a ring-shaped transformation hardening zone with a depth of 400 μm. Similar to the laser hardened specimen, apparent martensitic structure transformation occurred in this area, and the segregation degree of eutectic carbide was also reduced, as shown in Fig. 16c. The third one was the substrate, and its structure was mainly composed of pearlite and eutectic carbide, as given in Fig. 16d.

The microhardness distribution of LPH cross-section is shown in Fig. 17. The surface was heated by laser energy to produce considerable martensitic transformation, and the hardness of RZ was increased to 583 $HV_{500}$ because of the martensitic structure of fine grains, which was 133.2% higher than that of D2 tool steel. With the increase of depth, the influence of laser heating was smaller, and the microhardness diminished significantly. When the depth reached 0.7 mm, the microhardness tended to be stable at 250 $HV_{500}$. The results show that the depth of the hardened layer was 0.7 mm, which was consistent with the microstructure distribution (see Fig. 16a), where the EHZ depth was 0.24 mm and the HAZ depth was 0.46 mm.

Figure 18 presents the XRD pattern of D2 tool steel after LPH. Compared with the original material, in addition to the matrix phase α-Fe and the eutectic carbide $(Cr, Fe)_7C_3$, a new phase $(Cr_{2.5}Fe_{4.3}Mo_{0.1})C_3$ corresponding to the diffraction peaks (202), (402), and (412) was produced on the steel surface after laser treatment, which was roughly the same as those of the LP sample.

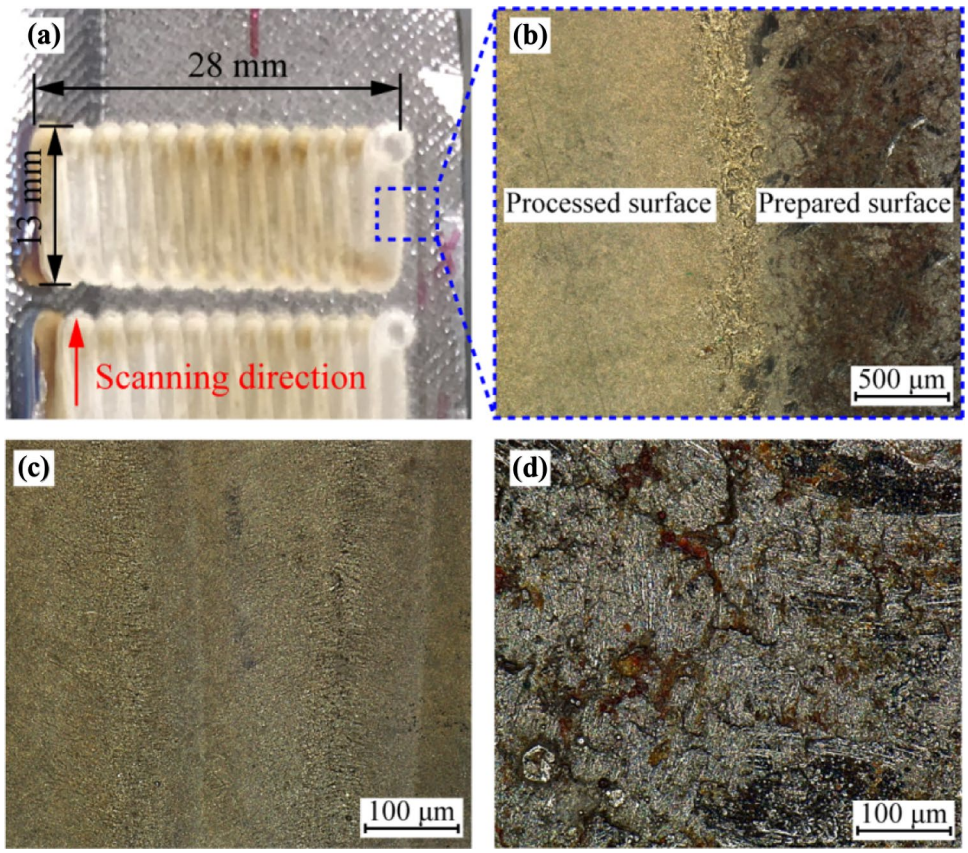


**Fig. 14** 3D surface morphologies of LPH specimen: (**a**) macroscopic image; (**b**) HOM image; (**c**), (**d**) higher-magnification HOM images of LPH and prepared surface

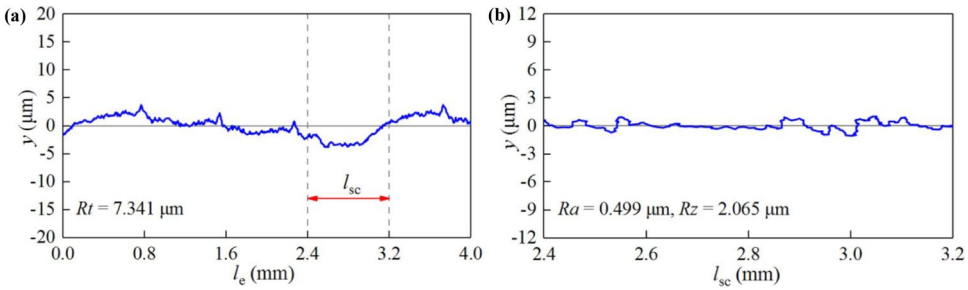


**Fig. 15** 2D surface morphologies of LPH specimen: (**a**) primary profile curve; (**b**) roughness profile curve

## 4 Discussions

### 4.1 Surface topography

Surface roughness has a remarkable influence on the deformation resistance and wear resistance of metallic materials. In this study, different laser processing approaches were used to reduce the surface roughness of D2 tool steel. In comparison with the initial milling surface, the surface roughness *Ra* obtained by LH method was only reduced by 5.7%, indicating that LH had a negligible effect on the surface topography of the tool steel. This is due to the laser energy used for LH was flat-top distribution, and the sample surface absorbed a small amount of uniform laser energy per unit area per unit time, thus melt material was not observed. While laser beams with Gaussian distribution were adopted in both LP and LPH experiments, the highly concentrated laser energy made the material surface heat up rapidly and melt. Moreover, due to the influence of surface tension, the convex part on the surface would flatten. With the removal of the laser beam, the molten material would solidify again, resulting in a significant reduction in the roughness of the processed surfaces. The surface roughness *Ra* of LP and LPH specimens decreased by 74.6% and 80.9%, respectively, demonstrating that the morphology of milled surface had been significantly improved, and especially LPH was more effective in reducing roughness.

Although the polishing mechanisms of LP and LPH were both to heat and melt the sample surface by laser application, resulting in the reduction of the initial surface roughness, the molten layer depth of the two processing methods was different due to diverse laser parameters applied in the experiments. The optimum laser energy density of LP test was 3333 J/cm$^2$, the defocus amount was 3 mm, and the energy acting on the specimen surface was small, which made the melting of the thin layer material on the surface, and the RZ depth was 30 μm, that is, the shallow melting mechanism. The optimal energy density used in the LPH experiment was 1786 J/cm$^2$ without defocus. Over melting of the surface was observed because considerable energy worked on the tool steel surface, and the RZ depth was 300 μm, that is, the over melting mechanism.

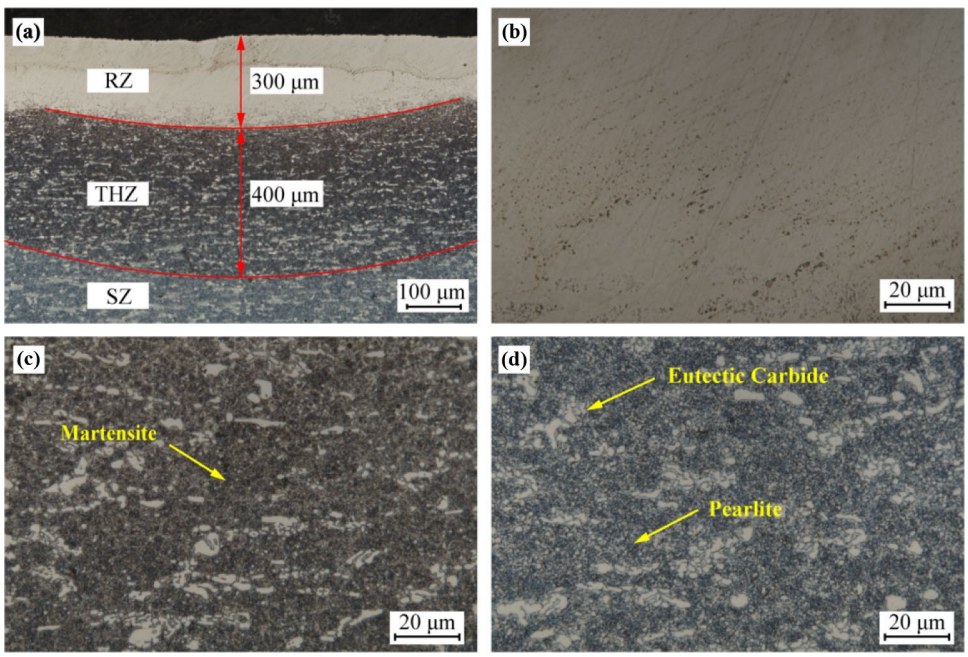


**Fig. 16** Cross-sectional microstructure using LPH: (**a**) overall; (**b**) RZ; (**c**) THZ; (**d**) SZ

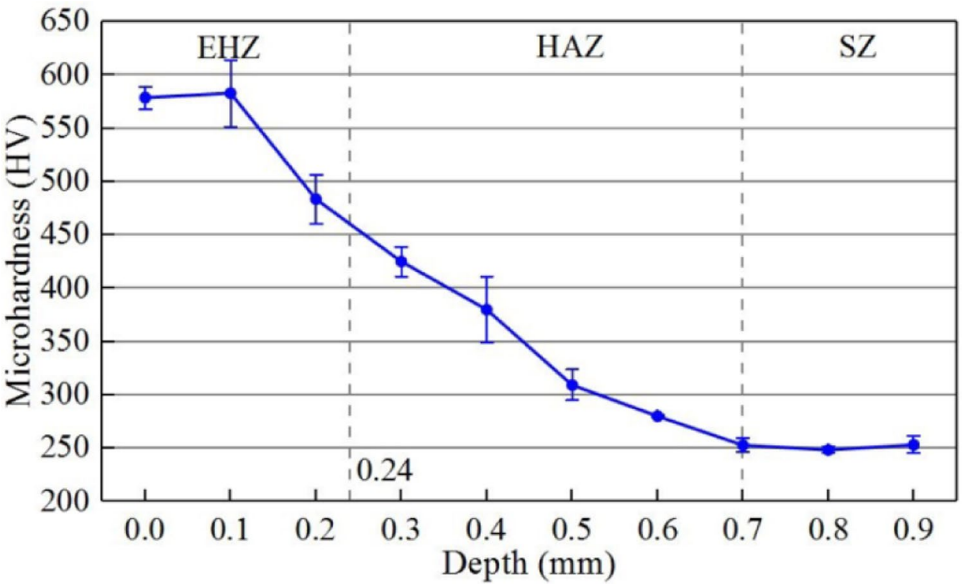


**Fig. 17** Microhardness distribution of LPH subsurface

In terms of polishing efficiency, a circular spot with a diameter of 0.1 mm was adopted in the LP experiment, and it took 150 min to polish a plane with the size of 100 mm × 100 mm. In the LPH test, the diameter of the laser beam was 2.8 mm, and it spent 15 min polishing a plane of the same size, indicating the treating efficiency was 10 times higher than that of LP. Moreover, the fastest time for reducing the original surface roughness by 80.9% was 30 min in the application of traditional polishing technologies such as magnetic grinding polishing, ultrasonic polishing, chemical polishing, electrolytic polishing, and fluid polishing. And metal polishing was performed by a skilled fitter, and it also took at least 120 min. Therefore, LPH has considerable advantages in polishing efficiency and is a very potential laser processing method for tool steel.

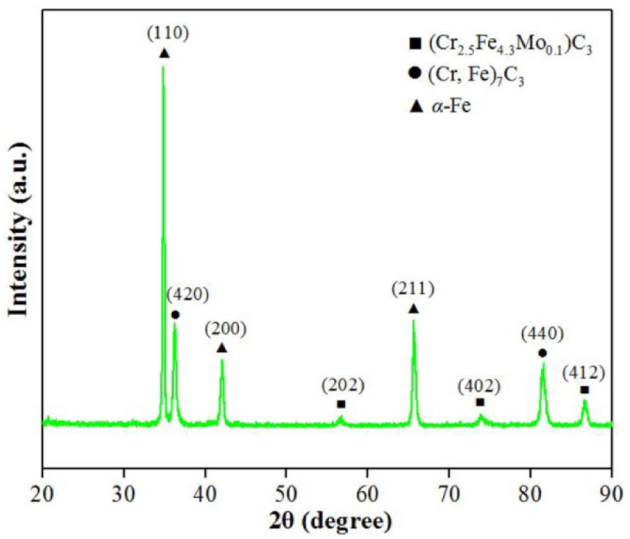


**Fig. 18** XRD pattern of D2 steel after LPH

## 4.2 Cross-section microhardness

The microhardness should be also considered an important parameter affecting the long-term properties of tool steel. Three laser processing processes were adopted to treat the surfaces of D2 tool steel. The results show that the LH and LPH approaches had a favorable effect on the cross-sectional hardness of D2 tool steel, while the increase of LP specimen on the microhardness was negligible. By observing the microstructure of the samples before and after laser treatments, it can be concluded that martensitic transformation plays a major role in improving the hardness of D2 tool steel. When the laser irradiates the sample surface, the material temperature reaches the austenitizing temperature, and the carbon diffuses outward from the transformation zone and enters the surrounding ferrite to form high-carbon austenite. The rapid cooling process leads to austenite nucleation and later growth, and D2 tool steel is easy to change into fine martensite due to its high carbon content. The surface material absorbed abundant laser energy during the LH test, then the structure changed into martensite with fine grains because of the rapid cooling, and thereby the microhardness increased to 634 $HV_{500}$, which was 2.5 times of the initial hardness. Besides, the uniformly distributed flat-top beam energy not only made the overall martensite evenly distributed but also made the microstructure of the material more compact. And the material thickness with the microhardness reaching the limiting hardness of D2 tool steel was 0.42 mm. In the LPH experiment, the surface of the processed sample was heated by the concentrated laser energy, which not only remelted the material and reduced the surface roughness

but also occurred completely martensitic transformation. The martensitic structure of fine grains increased the hardness of RZ to 583 $HV_{500}$, which was 1.3 times higher than the initial hardness, and the depth of the effective hardening layer was 0.24 mm.

The phase composition changes of D2 steel treated by different laser processing methods were studied. The results illustrate that a new phase secondary carbide $(Cr_{2.5}Fe_{4.3}Mo_{0.1})C_3$ was produced on the steel surface after three laser treatments, except for the matrix phase $\alpha$-Fe and eutectic carbide $(Cr, Fe)_7C_3$ contained in the original material. Moreover, due to the lack of shielding gas in the LH experiment, an oxidation reaction occurred to produce oxide $Fe_2O_3$. The PDF standard card of XRD shows that $(Cr_{2.5}Fe_{4.3}Mo_{0.1})C_3$ and $(Cr, Fe)_7C_3$ are the same hexagonal structure, and both are $M_7C_3$ carbides. From the crystallographic point of view, secondary $(Cr_{2.5}Fe_{4.3}Mo_{0.1})C_3$ can be regarded as formed by the substitution of some Fe atoms by Mo atoms in primary $(Cr, Fe)_7C_3$, and the lattice distortion of carbides leads to the change of lattice constant. The solid solution of Cr in the matrix is another strengthening mechanism to improve the hardness of D2 tool steel. With the laser heat source close to the surface of D2 steel, the heated area rises rapidly. When the temperature reaches the melting point of eutectic carbide, it is caused by the partial dissolution of $(Cr, Fe)_7C_3$, which is also the reason for the reduction of eutectic carbide size after laser treatments. The solute atoms incorporated into the solid solution cause lattice distortion, which increases the resistance of dislocation movement and makes it difficult to slip, leading to the improvement of the hardness of D2 steel solid solution.

## 5 Conclusions

This work proposed a high-efficient laser polishing-hardening technology for the treatment of AISI D2 tool steel surface and studied the influences of LH, LP, and LPH approaches on surface topography and cross-sectional microhardness.

LH method had a negligible effect on the surface roughness of the treated sample, while the surface roughness *Ra* of LP and LPH specimens was reduced by 74.6% and 80.9%, respectively, indicating that the milled surface topography had been significantly improved, and especially LPH was more effective in reducing the roughness. Moreover, the polishing efficiency of LPH was 10 times that of the LP approach.

In the LP test, the laser energy acting on the sample surface was small, which made the surface thin layer material melt, and the RZ depth was 30 μm, that is, shallow melting mechanism. In the LPH experiment, considerable energy acted on the surface of tool steel. It was observed that the surface was over melted, and the RZ depth was 300 μm, that is, over melting mechanism.

Martensitic transformation and solution strengthening of Cr play a major role in improving the hardness of D2 tool steel. The near-surface microhardness of LH and LPH samples increased by 1.5 times and 1.3 times, respectively, and the effective hardened layer depth was 0.42 mm and 0.24 mm, respectively, demonstrating that these two laser processing methods had a beneficial effect on the cross-section microhardness of D2 tool steel, while the increase of LP on the microhardness was insignificant.

LPH was a feasible laser surface treatment method for D2 tool steel. On the premise of ensuring a high surface finish, LPH method not only remarkably improved the polishing efficiency, but also significantly increased the subsurface microhardness and EHZ depth of processed specimen, which provided an effective idea for the application of laser surface treatment technology in industrial mold production.

However, the higher the hardness of metallic materials, the greater the plastic deformation resistance and the higher the yield strength, but the toughness usually reduces with the rise of hardness. Telasang et al. [26] studied the laser surface hardening of AISI H13 hot working tool steel by adopting a diode laser. They found that the yield strength of the remelted material on the treated sample surface was significantly improved, but the fatigue strength was remarkably lower than that of the initial material due to the brittle structure of carbide precipitation at the grain boundary. It is well-known that automobile stamping dies not only need high hardness to improve the ability to resist plastic deformation, but also need good toughness to increase the ability to resist fracture. Therefore, to satisfy the functional requirements of stamping die, potential mechanical behavior changes must also be considered. In the follow-up investigation, the mechanical properties (such as yield strength, fatigue strength, wear resistance) and strengthening mechanism (such as grain boundary strengthening and precipitation strengthening) of the remelted materials of LPH samples will be studied to further verify the feasibility and effectiveness of the developed laser polishing-hardening approach.

**Author contribution** Zuofa Liu, Hang Wang, and Jie Zhou conceived and designed the study. Zuofa Liu, Hang Wang, Qiuyun Wang, and Yongliang Li performed the experiments. Jie Zhou provided funding. Zuofa Liu and Qiang Liang wrote the paper. Hang Wang, Qiuyun Wang, Yongliang Li, and Jie Zhou reviewed and edited the manuscript. All authors read and approved the manuscript.

**Funding** This research was supported by the National Natural Science Foundation of China (52075058), Science and Technology Project of Guizhou Province (Qiankehe Support [2021] General 308), and Chongqing Graduate Scientific Research and Innovation Foundation (CYS21003).

**Data availability** All data, models, and code generated or used during the study appear in the submitted article.

## Declarations

**Consent to publish** All authors agree to publication in The International Journal of Advanced Manufacturing Technology.

**Competing interests** The authors declare no competing interests.

## References


1. Peng Y, Shen B, Wang Z, Yang P, Yang W, Bi G (2021) Review on polishing technology of small-scale aspheric optics. Int J Adv Manuf Technol 115(4):965–987. https://doi.org/10.1007/s00170-021-07202-3
2. Wu Y (2017) Research on laser quenching process of automobile stamping die steel Cr12MoV and wear mechanism. Dissertation, Shenyang University of Technology
3. Shu Q, Zhou J, Peng S, Wang Q, Zhang J (2022) Study on microstructure of laser cladding fe-based coatings and comparison of mechanical properties with SKD11 steel. Trans Indian Inst Met 75(1):35–46. https://doi.org/10.1007/s12666-021-02392-6
4. Krishnan A, Fang F (2019) Review on mechanism and process of surface polishing using lasers. Front Mech Eng 14(3):299–319. https://doi.org/10.1007/s11465-019-0535-0
5. Dai W, Li J, Zhang W, Zheng Z (2019) Evaluation of fluences and surface characteristics in laser polishing SKD 11 tool steel. J Mater Process Technol. https://doi.org/10.1016/j.jmatprotec.2019.05.022
6. Ukar E, Lamikiz A, Martínez S, Tabernero I, Lacalle L (2012) Roughness prediction on laser polished surfaces. J Mater Process Technol 212(6):1305–1313
7. Ukar E, Lamikiz A, López de Lacalle LN, del Pozo D, Arana JL (2010) Laser polishing of tool steel with CO2 laser and high-power diode laser. Int J Mach Tools Manuf 50(1):115–125. https://doi.org/10.1016/j.ijmachtools.2009.09.003
8. Chang C-S, Chen T-H, Li T-C, Lin S-L, Liu S-H, Lin J-F (2016) Influence of laser beam fluence on surface quality, microstructure, mechanical properties, and tribological results for laser polishing of SKD61 tool steel. J Mater Process Technol 229:22–35. https://doi.org/10.1016/j.jmatprotec.2015.09.009
9. Guo W, Hua M, Tse PW-T, Mok ACK (2012) Process parameters selection for laser polishing DF2 (AISI O1) by Nd:YAG pulsed laser using orthogonal design. Int J Adv Manuf Technol 59(9–12):1009–1023. https://doi.org/10.1007/s00170-011-3558-1
10. Ma CP, Guan YC, Zhou W (2017) Laser polishing of additive manufactured Ti alloys. Opt Lasers Eng 93:171–177. https://doi.org/10.1016/j.optlaseng.2017.02.005
11. Pong-Ryol J, Tae-Sok J, Nam-Chol K, Xing F, kum-Hyok J (2015) Laser micro-polishing for metallic surface using UV nano-second pulse laser and CW laser. Int J Adv Manuf Technol 85(9–12):2367–2375. https://doi.org/10.1007/s00170-015-7992-3
12. Kang D, Zou P, Wu H, Wang W, Xu J (2021) Research on ultrasonic vibration-assisted laser polishing of the 304 stainless steel. J Manuf Process 62:403–417. https://doi.org/10.1016/j.jmapro.2020.12.009
13. Zhou H, Zhou H, Zhao Z, Li K, Yin J (2021) Numerical simulation and verification of laser-polishing free surface of S136D die steel. Metals 11(3). https://doi.org/10.3390/met11030400
14. Lee S, Ahmadi Z, Pegues JW, Mahjouri-Samani M, Shamsaei N (2021) Laser polishing for improving fatigue performance of additive manufactured Ti-6Al-4V parts. Opt Laser Technol. https://doi.org/10.1016/j.optlastec.2020.106639
15. Muthukumaran G, Babu PD (2021) Metallurgical characterization of laser hardened, mechanically textured 2.5 Ni-Cr-Mo low alloy steel and optimization using RSM. Opt Laser Technol 141. https://doi.org/10.1016/j.optlastec.2021.107126
16. Bande H, L'Espérance G, Islam MU, Koul AK (2013) Laser surface hardening of AISI 01 tool steel and its microstructure. Mater Sci Technol 7(5):452–457. https://doi.org/10.1179/mst.1991.7.5.452
17. Akao T, Sakurai Y, Onda T, Uehara K, Chen Z-C (2014) Surface modification of cold-working die steel by electron beam irradiation – formation of cemented carbide composite layer. Procedia Engineering 81:1939–1944. https://doi.org/10.1016/j.proeng.2014.10.261
18. Amine T, Newkirk JW, El-Sheikh HE-DF, Liou F (2014) Microstructural and hardness investigation of tool steel D2 processed by laser surface melting and alloying. Int J Adv Manuf Technol 73(9–12):1427–1435. https://doi.org/10.1007/s00170-014-5882-8
19. Chen C, Zeng X, Wang Q, Lian G, Huang X, Wang Y (2020) Statistical modelling and optimization of microhardness transition through depth of laser surface hardened AISI 1045 carbon steel. Opt Laser Technol. https://doi.org/10.1016/j.optlastec.2019.105976
20. Lesyk DA, Martinez S, Dzhemelinskyy VV, Lamikiz A, Mordyuk BN, Prokopenko GI (2015) Surface microrelief and hardness of laser hardened and ultrasonically peened AISI D2 tool steel. Surf Coat Technol 278:108–120. https://doi.org/10.1016/j.surfcoat.2015.07.049
21. Li R, Jin Y, Li Z, Qi K (2014) A comparative study of high-power diode laser and CO2 laser surface hardening of AISI 1045 steel. J Mater Eng Perform 23(9):3085–3091. https://doi.org/10.1007/s11665-014-1146-x
22. Dinesh Babu P, Buvanashekaran G, Balasubramanian KR (2012) Experimental investigation of laser transformation hardening of low alloy steel using response surface methodology. Int J Adv Manuf Technol 67(5–8):1883–1897. https://doi.org/10.1007/s00170-012-4616-z
23. Lee J-H, Jang J-H, Joo B-D, Son Y-M, Moon Y-H (2009) Laser surface hardening of AISI H13 tool steel. Trans Nonferrous Metals Soc China 19(4):917–920. https://doi.org/10.1016/s1003-6326(08)60377-5
24. Tobar MJ, Álvarez C, Amado JM, Ramil A, Saavedra E, Yáñez A (2006) Laser transformation hardening of a tool steel: simulation-based parameter optimization and experimental results. Surf Coat Technol 200(22–23):6362–6367. https://doi.org/10.1016/j.surfcoat.2005.11.067
25. Ramos-Grez JA, Bourell DL (2004) Reducing surface roughness of metallic freeform-fabricated parts using non-tactile finishing methods. Int J Mater Prod Technol 21(4):297–316. https://doi.org/10.1504/ijmpt.2004.004944
26. Telasang G, Dutta Majumdar J, Padmanabham G, Manna I (2014) Structure–property correlation in laser surface treated AISI H13 tool steel for improved mechanical properties. Mater Sci Eng A 599:255–267. https://doi.org/10.1016/j.msea.2014.01.083